




Article

# On the Prospects of Multiport Devices for Photon-Number-Resolving Detection

Yong Siah Teo <sup>1,\*</sup>, Hyunseok Jeong <sup>1</sup>, Jaroslav Řeháček <sup>2</sup>, Zdeněk Hradil <sup>2</sup>, Luis L. Sánchez-Soto <sup>3,4</sup> and Christine Silberhorn <sup>5</sup>

<sup>1</sup> Department of Physics and Astronomy, Seoul National University, Seoul 08826, Korea; jeongh@snu.ac.kr

<sup>2</sup> Department of Optics, Palacký University, 17. listopadu 12, 77146 Olomouc, Czech Republic; rehacek@optics.upol.cz (J.Ř.); hradil@optics.upol.cz (Z.H.)

<sup>3</sup> Max-Planck-Institut für die Physik des Lichts, Staudtstraße 2, 91058 Erlangen, Germany; lsanchez@ucm.es

<sup>4</sup> Departamento de Óptica, Facultad de Física, Universidad Complutense, 28040 Madrid, Spain

<sup>5</sup> Integrated Quantum Optics Group, Applied Physics, University of Paderborn, 33098 Paderborn, Germany; christine.silberhorn@upb.de

\* Correspondence: ys\_teo@snu.ac.kr

Received: 10 September 2019; Accepted: 26 September 2019; Published: 29 September 2019



**Abstract:** Ideal photon-number-resolving detectors form a class of important optical components in quantum optics and quantum information theory. In this article, we theoretically investigate the potential of multiport devices having reconstruction performances approaching that of the Fock-state measurement. By recognizing that all multiport devices are minimally complete, we first provide a general analytical framework to describe the tomographic accuracy (or quality) of these devices. Next, we show that a perfect multiport device with an infinite number of output ports functions as either the Fock-state measurement when photon losses are absent or binomial mixtures of Fock-state measurements when photon losses are present and derive their respective expressions for the tomographic transfer function. This function is the scaled asymptotic mean squared error of the reconstructed photon-number distributions uniformly averaged over all distributions in the probability simplex. We then supply more general analytical formulas for the transfer function for finite numbers of output ports in both the absence and presence of photon losses. The effects of photon losses on the photon-number resolving power of both infinite- and finite-size multiport devices are also investigated.

**Keywords:** photon-number-resolving detectors; multiport devices; quantum optics; Fock states; quantum tomography; photon losses

## 1. Introduction

Photon-number-resolving (PNR) detection schemes are measurements that play a vital role in quantum information theory. The ability to perform direct photon counting has been shown to fundamentally impact quantum protocols and technologies. These include quantum metrology [1–4], quantum key distribution [5,6], Bell measurements [7] and quantum random number generator [8,9]. In practice, such PNR measurements either do not faithfully resolve photon numbers or do so up to a limited (typically small) number of photons, especially in the emblematic presence of dark counts and photon losses [10,11]. In recent years, there has been significant progress in the quality and type of photon-counting detectors developed through new-generation quantum engineering techniques [12–19].

An alternative class of setups that are widely used to indirectly perform photon counting are the so-called multiport devices [20–22], which are schematically more sophisticated devices that involve

multiple beam splitters and several output ports that lead to “on-off” photodetectors for counting the number of split output signal pulses. Such alternative devices are later refashioned using optical-fiber looping [23,24] or multiplexing [25–28] strategies that give exactly the same photon-number-resolving characteristics but with much more efficient and cost-effective architectures.

In this article, we invoke the machinery of quantum tomography to evaluate the performance of general multiport devices. After providing the general descriptions of multiport devices in Section 2 and introducing the concept of informational completeness for such commuting measurements in Section 3, we establish a general framework in Section 4 to certify their tomographic performances using an operational tomographic transfer function that measures the average asymptotic accuracies of reconstructed photon-number distributions (Equation (33)). According to this formalism, we first investigate the performances of multiport devices that have infinitely many output ports with and without photon losses in Section 5. We shall show respectively that these infinitely large devices behave either exactly like a set of Fock-state measurement outcomes or their binomial-noisy mixtures and derive their tomographic transfer functions (Equations (40) and (49)). We will also demonstrate in Section 5.3 that photon losses can severely limit the photon-number resolution of multiport devices and systematically characterize such limitations in terms of informational completeness phase diagrams and the dependence of the maximum photon-loss rate tolerable on the number of photons to be resolved. Finally in Section 6, we shall derive general formulas for the transfer functions for the most general multiport devices with finite output ports (Equations (58) and (60)) and evaluate the effects of photon losses on their photon-number resolving power in Section 6.3.

## 2. General Physics of Multiport Devices

A multiport device is general laboratory equipment that houses an input port for receiving photonic signals and a fixed number (say  $s$ ) of output ports. After undergoing multiple splitting of an input photonic pulse inside the device, each output port would then either idle (symbolically labeled as “0”) or register a photonic “click” (“1”) that originates from the split pulse. As an example, a three-port device would contain  $s = 3$  output ports that give a total of  $2^3 = 8$  different detection configurations, which are the “000”, “001”, “010”, “100”, “011”, “101”, “110” and “111” detection events. For the purpose of photon-number-distribution reconstruction, we may as well consolidate all the “0-click”, “1-click”, “2-click” and “3-click” events respectively and describe this multiport device as a measurement of  $M = 4$  outcomes. More generally, an  $s$ -port device is one that gives  $2^s$  detection configurations that may be organized to yield a total of  $M = s + 1$  measurement events.

Any measurement can be described by a *positive operator-valued measure* (POVM), a set of probability operators (outcomes) that is given by

$$\Pi_j \geq 0 \quad \text{such that} \quad \sum_{j=0}^{M-1} \Pi_j = 1. \quad (1)$$

A multiport device is no exception, and is therefore mathematically equivalent to a POVM of  $M = s + 1$  outcomes, where a “ $j$ -click” outcome is some unnormalized mixture  $\Pi_j = \sum_n |n\rangle \beta_{jn} \langle n|$  of Fock states. For a sufficiently large number of data sampling events  $N$ , the data obtained from a measurement of such a POVM give probabilities that are linear combinations of the expectation values  $\langle |n\rangle \langle n| \rangle$ . The photon-number distribution can subsequently be reconstructed. The amplitudes  $\beta_{jn}$  are, in general, complicated functions of all the port efficiencies  $\{\eta_j\}$  ( $\sum_j \eta_j \leq 1$ ), each of which depends on the physical parameters of the actual device implementation such as beam-splitter ratio, photodetector efficiency, and so on.

In particular, for arbitrary port efficiencies  $\sum_j \eta_j \equiv 1 - \epsilon$ , the “0-click” outcome  $\Pi_0$  possesses amplitudes  $\beta_{0,n} = \epsilon^n$  that are independent of any other detail of the multiport specifications. In other words, the probability of a “0-click” event for an  $n$ -photon input signal is the  $n$ -fold product of the loss probability  $\epsilon$ , which is consistent with the physical fact that photoabsorption and detector losses

are the main mechanisms behind all “0-click” events when  $n > 0$  in the absence of other kinds of experimental imperfections.

If the light source is effectively described by a quantum state  $\rho$  in a Hilbert space of dimension  $d$ , so that the probability of detecting  $n > d - 1$  photons is practically zero, then all “( $j > d - 1$ )-click” outcomes are correspondingly zero by construction. The outcomes  $\Pi_j$  are hence represented by  $d \times d$  positive matrices that sum to the identity matrix. We can define the measurement matrix that concisely and uniquely determine the multiport POVM. To do this, we first emphasize that in this effective Hilbert space, the conditional photon-number probabilities  $\rho_n = \langle n | \rho | n \rangle = \langle |n\rangle \langle n|$  are properly normalized ( $\text{tr}\{\rho\} = 1$ ), so that the total number of independent parameters to be estimated is  $d - 1$ . From Born’s rule, we may express the multiport probabilities in terms of  $d - 1$  independent state parameters inasmuch as

$$p_j = \text{tr}\{\rho\Pi_j\} = \sum_{n=0}^{d-2} (\beta_{jn} - \beta_{jd-1})\rho_n + \beta_{jd-1}. \tag{2}$$

Following the reasonings in quantum-state tomography [29,30], we may define the measurement matrix

$$C = \sum_{j=0}^{d-1} \sum_{n=0}^{d-2} e_j e_n (\beta_{jn} - \beta_{jd-1}), \tag{3}$$

with the help of the standard computational basis  $e_l \cdot e_{l'} = \delta_{l,l'}$ , to be the  $d \times (d - 1)$  rectangular matrix that fully characterizes the multiport POVM for the  $d - 1$  independent  $\rho_n$  parameters. It is clear that this matrix has a zero eigenvalue corresponding to the eigenvector  $\mathbf{1}_d$  that is represented as a  $d$ -dimensional column of ones— $\mathbf{1}_d \cdot C = \mathbf{0}_{d-1}^T$ .

We shall look into an interesting special case where the port efficiencies are all equal to a constant ( $\eta_j = \eta$ ), so that the POVM amplitudes can be shown to take the simple form [20,23,25]

$$\beta_{jn} = (-1)^j \binom{s}{j} \sum_{k=0}^j \binom{j}{k} (-1)^k [1 - \eta(s - k)]^n. \tag{4}$$

The self-consistent consequence  $\sum_{j=0}^s \beta_{jn} = 1$  can be verified straightforwardly. This type of multiport device is commonly used in practice. We mention in passing that the outcomes  $\Pi_j$  may be equivalently expressed as the normal-ordered form

$$\Pi_j = \binom{s}{j} : (e^{-\eta a^\dagger a})^{s-j} (1 - e^{-\eta a^\dagger a})^j : \tag{5}$$

from which Equation (4) is quickly obtained through the application of the formula

$$: F(a^\dagger a) : = F\left(\frac{d}{dx}\right) x^{a^\dagger a} \Big|_{x=1}, \tag{6}$$

for any operator function  $F(a^\dagger a)$  of the number operator  $a^\dagger a$ .

Dark counts may be incorporated in a simplistic way by introducing the parameter  $\nu > 0$  that defines the average dark-count rate as the transformation  $\eta a^\dagger a \rightarrow \eta a^\dagger a + \nu$  to Equation (5). Physically, this transformation increases the partially-depleted number operator  $\eta a^\dagger a$  due to losses by an additional  $\nu$  photons on average. In what follows, dark-count rates are assumed to be negligible in the feasible bandwidth of the photodetectors.

### 3. Informational Completeness of Photon-Number Distribution Measurements

To analyze photon-number-distribution reconstruction with multiport devices, we shall review the tools that are employed in understanding quantum measurements in this context. We recall that

an informationally complete (IC) measurement is one that uniquely characterizes a particular set of physically relevant parameters describing a given quantum source of interest. In quantum-state tomography, such a measurement unambiguously reconstructs the quantum state  $\rho$  for the source. For our purpose, the set of parameters constitutes the photon-number distribution  $\{\rho_n\}$  of a quantum light source, which are the diagonal entries of  $\rho$  in the Fock basis as mentioned in Section 2. With respect to the  $\rho_n$ s, a POVM is IC when it contains at least  $d$  outcomes with a degree of linear independence of  $d$ .

The entire machinery for IC quantum-state tomography can be translated for photon-number distribution tomography. The concept of the operator ket is particularly helpful here for notational simplification. For any  $d$ -dimensional operator  $O$  in the Fock basis, its operator ket  $|O\rangle$  is defined as the  $d$ -dimensional column vector of its diagonal entries. The photon-number distribution of  $\rho$  that is of interest to us is thus summarized by its operator ket  $|\rho\rangle$  such that  $\text{tr}\{\rho\} = \langle 1|\rho\rangle = 1$ . With this, we can define the frame operator

$$\mathcal{F} = \sum_{j=0}^{M-1} \frac{|\Pi_j\rangle\langle\Pi_j|}{\text{tr}\{\Pi_j\}}, \tag{7}$$

for any POVM  $\{\Pi_j\}$  comprising  $M$  commuting Fock-state mixtures. Hence, an equivalent definition for an IC POVM is the operator invertibility of  $\mathcal{F}$ . In addition, using the operator-ket notation, the degree of linear independence of the POVM can be checked by inspecting the eigenvalues of the standard Gram matrix

$$\mathbf{G} = \sum_{j=0}^{M-1} \sum_{k=0}^{M-1} e_j e_k \langle\Pi_j|\Pi_k\rangle = \mathbf{V}\mathbf{V}^\dagger, \quad \mathbf{V} = \begin{pmatrix} \langle\Pi_1| \\ \vdots \\ \langle\Pi_M| \end{pmatrix}, \tag{8}$$

for vectorial objects.

For multiport devices, Equation (7) is applicable for  $M = s + 1$ . Consequently, it is necessary for the corresponding multiport POVM to have  $s \geq d - 1$  output ports for it to be IC in a  $d$ -dimensional Hilbert space. Moreover, there exists another important feature for these devices. As discussed in Section 2, that the probability of detecting more photons than the number available in the input signal is zero implies that any multiport POVM is necessarily minimally complete when it is IC on the  $d$ -dimensional Hilbert space. This means that for such minimal POVMs, there are effectively only  $M = d$  nonzero outcomes (each having amplitudes that depend on  $s$ ) and we can uniquely express the photon-number distribution as

$$|\rho\rangle = \sum_{j=0}^{d-1} |\Theta_j\rangle p_j \tag{9}$$

with the help of the  $d$  canonical dual operators

$$|\Theta_j\rangle = \mathcal{F}^{-1} \frac{|\Pi_j\rangle}{\text{tr}\{\Pi_j\}}. \tag{10}$$

It can be shown that

$$\langle\Pi_j|\Theta_k\rangle = \delta_{j,k} \tag{11}$$

for any minimal POVM. For this, we use the general property

$$\mathbf{W}^\dagger \mathbf{V} = \mathbf{1} = \mathbf{V}^\dagger \mathbf{W}, \quad \mathbf{W} = \begin{pmatrix} \langle\Theta_1| \\ \vdots \\ \langle\Theta_M| \end{pmatrix}, \tag{12}$$

for any set of (canonical) dual operators, so that sandwiching the left equation in (12) with  $\mathbf{V}$  from the left and  $\mathbf{V}^\dagger$  from the right gives

$$VW^\dagger G = G = GWV^\dagger. \tag{13}$$

Next, we realize that for any minimal POVM,  $G$  is always invertible and we have  $VW^\dagger = 1 = WV^\dagger$ .

#### 4. General Framework for the Reconstruction Accuracy of Multiport Devices

##### 4.1. Mean Squared-Error and Its Cramér–Rao Bound

We shall take the mean squared-error (MSE)  $\mathcal{D}_{\text{MSE}}$  as the measure of the reconstruction accuracy of the photon-number distribution  $|\rho\rangle$ . For a given estimator  $|\hat{\rho}\rangle$  of  $|\rho\rangle$ , since only  $\rho_n \big|_{n=0}^{d-2}$  are independent, this measure is defined as

$$\mathcal{D}_{\text{MSE}} = \mathbb{E}_{\text{data}}[(|\hat{\rho}\rangle - |\rho\rangle)^2] \Big|_{\text{supp}}, \tag{14}$$

where the average is taken over all plausible data. The label “supp” means that the inner product is evaluated in the  $(d - 1)$ -dimensional support of the linearly independent parameters of  $|\rho\rangle$ . The parameter space of  $|\rho\rangle$  is the entire  $d$ -dimensional probability simplex, since one can always find a quantum state  $\rho$  that gives any particular  $|\rho\rangle$  (a statistical mixture of Fock states weighted with the  $\rho_{ns}$ , for instance). The boundary of this space is therefore the edges of this simplex.

When  $|\rho\rangle$  is off the boundary ( $\rho_n \neq 0$ ), which is the real experimental situation, it is well-known that the scaled MSE with  $N$  is bounded from below by the Cramér–Rao bound (CRB) per sampling event,

$$N\mathcal{D}_{\text{MSE}} \geq \text{tr}\{F(\rho)^{-1}\}, \tag{15}$$

where  $F(\rho)$  is the  $(d - 1)$ -dimensional Fisher information operator (defined per sampling event) for a given  $|\rho\rangle$  and POVM. In particular, the unbiased maximum-likelihood (ML) estimator saturates this bound asymptotically in the limit of large  $N$ . Boundary  $|\rho\rangle$ s may be included in the picture by taking appropriate limits. The CRB directly evaluates the reconstruction accuracy of  $|\rho\rangle$  where the constraint  $\text{tr}\{\rho\} = \langle 1|\rho\rangle = 1$  is obeyed, and supplies the limit of photon-number reconstruction for any  $|\rho\rangle$ .

For any minimal POVM, the MSE has a simple compact form for single-shot experiments that yield multinomial data statistics, just as for any multiport device. First, we can define the linear estimator of  $|\rho\rangle$ , in terms of the canonical dual operators and the measured multiport relative frequencies  $v_j$ , as

$$|\hat{\rho}\rangle = \sum_{j=0}^{d-1} |\Theta_j\rangle v_j, \tag{16}$$

where  $\langle \Pi_j|\rho\rangle = v_j$  for any minimal POVM. The fact that  $\mathbb{E}_{\text{data}}[|\hat{\rho}\rangle] = |\rho\rangle$  is evident. Second, we recall that this linear estimator is in fact the ML estimator whenever  $|\rho\rangle > \mathbf{0}$  for sufficiently large  $N$ , so that the linear estimator in Equation (16) saturates the CRB. So, using the identity

$$\mathbb{E}_{\text{data}}[v_j v_k] = \frac{1}{N} [\delta_{j,k} p_j + (N - 1) p_j p_k], \tag{17}$$

for multinomial distributions, we have

$$\begin{aligned} \mathcal{D}_{\text{MSE}} &= \mathbb{E}_{\text{data}}[\langle \hat{\rho}|\hat{\rho}\rangle] - \langle \rho|\rho\rangle \Big|_{\text{supp}} \\ &= \sum_{j=0}^{d-1} \sum_{k=0}^{d-1} \langle \Theta_j|\Theta_k\rangle (\mathbb{E}_{\text{data}}[v_j v_k] - p_j p_k) \Big|_{\text{supp}} \\ &= \frac{1}{N} \left( \sum_{j=0}^{d-1} \langle \Theta_j|\Theta_j\rangle p_j - \langle \rho|\rho\rangle \right) \Big|_{\text{supp}}. \end{aligned} \tag{18}$$

On the other hand for multinomial data statistics, it is known that the Fisher operator takes the form

$$\begin{aligned} F(|\rho\rangle) &= \sum_{l=0}^{d-1} (|\Pi_l\rangle - |1\rangle \beta_{l,d-1}) \frac{1}{p_l} (\langle \Pi_l | - \beta_{l,d-1} \langle 1 |) \Big|_{\text{supp}} \\ &= \mathbf{C}^T \mathbf{P}^{-1} \mathbf{C}, \end{aligned} \tag{19}$$

where  $\mathbf{P}_j = p_j$ . In view of this, we arrive at the identity

$$\begin{aligned} \text{tr}\{F(|\rho\rangle)^{-1}\} &= \text{tr}\{(\mathbf{C}^T \mathbf{P}^{-1} \mathbf{C})^{-1}\} \\ &= \left( \sum_{j=0}^{d-1} \langle \Theta_j | \Theta_j \rangle p_j - \langle \rho | \rho \rangle \right) \Big|_{\text{supp}} \end{aligned} \tag{20}$$

for any minimal POVM with respect to the photon-number distribution.

#### 4.2. A Measure of Tomographic Performance

The CRB in Equation (20) is a function of  $|\rho\rangle$ . To obtain an operational performance certifier, one may choose to average over  $|\rho\rangle$ , which can be carried out in many different ways. We shall follow a similar direction reported in ref. [30] and perform an average over all distributions over the probability simplex. The resulting average CRB

$$\text{TTF} = \mathbb{E}_{|\rho\rangle} [\text{tr}\{F(|\rho\rangle)^{-1}\}] \tag{21}$$

is the tomographic transfer function (TTF) for photon-number distributions, which generalizes previous analytical scopes, such as those in [11,22], that focus on the class of Poissonian distributions to other more exotic yet classically allowed probability distributions  $\{p_j\}$  in the  $(d - 1)$ -dimensional simplex. Following through the calculations, using the simplex identities (see Appendix B)

$$\mathbb{E}_{|\rho\rangle} [p_j] = \frac{1}{d} \quad \text{and} \quad \mathbb{E}_{|\rho\rangle} [p_j^2] = \frac{2}{d(d+1)}, \tag{22}$$

we have

$$\mathbb{E}_{|\rho\rangle} [\langle \rho | \rho \rangle] \Big|_{\text{supp}} = \sum_{n=0}^{d-2} \mathbb{E}_{|\rho\rangle} [p_n^2] = \frac{2(d-1)}{d(d+1)}. \tag{23}$$

$$\text{TTF}_{\text{multiport}} = \mathbb{E}_{|\rho\rangle} [\text{tr}\{F(|\rho\rangle)^{-1}\}] = \frac{1}{d} \text{tr}\{\mathcal{F}^{-1}\} \Big|_{\text{supp}} - \frac{2(d-1)}{d(d+1)}. \tag{24}$$

Finally it turns out that Equation (24) may also be obtained from an average of  $F(|\rho\rangle)$  uniformly (under the Haar measure) over all pure states  $\rho$ , after a reference to Equation (10).

One can proceed to express the first term on the rightmost side of Equation (24) by recognizing that

$$\text{tr}\{\mathcal{F}^{-1}\} \Big|_{\text{supp}} = \text{tr}\{\mathcal{F}^{-1}\} - \langle d-1 | \mathcal{F}^{-1} | d-1 \rangle, \tag{25}$$

and that the Fock state

$$|d-1\rangle = \frac{|\Pi_{d-1}\rangle}{\text{tr}\{\Pi_{d-1}\}} \tag{26}$$

for any multiport device since in the absence of dark counts, the “ $j$ -click” event occurs when there are  $j$  photons or more. Then the orthonormality property in Equation (11) dictates that

$$\langle d-1 | \mathcal{F}^{-1} | d-1 \rangle = \frac{1}{\text{tr}\{\Pi_{d-1}\}^2} \langle \Pi_{d-1} | \mathcal{F}^{-1} | \Pi_{d-1} \rangle = \frac{1}{\text{tr}\{\Pi_{d-1}\}}, \tag{27}$$

which brings us to the slightly more explicit expression

$$\text{TTF}_{\text{multiport}}(s, \{\eta_j\}) = \frac{1}{d} \text{tr}\{\mathcal{F}^{-1}\} - \frac{1}{d \text{tr}\{\Pi_{d-1}\}} - \frac{2(d-1)}{d(d+1)}. \tag{28}$$

The result in Equation (33) assigns a number to the average performance of a multiport device of arbitrary number of output ports  $s$ , port efficiencies  $\{\eta_j\}$  and loss probability  $\epsilon$  based on statistical estimation theory.

For any multiport POVM of amplitudes  $\beta_{jn}$ , by defining  $\mathbf{B}_{s,\epsilon}$  to be the square matrix of these amplitudes  $(\mathbf{B}_{s,\epsilon})_{jn} = \beta_{jn}$ , the operator kets  $|\Pi_j\rangle$  and the Fock kets  $|n\rangle$  are then related by the simple linear system

$$\mathbf{V} = \mathbf{B}_{s,\epsilon} \mathbf{v}, \quad \mathbf{v} = \begin{pmatrix} \langle 0| \\ \vdots \\ \langle d-1| \end{pmatrix}, \tag{29}$$

where the column  $\mathbf{V}$  of operator bras is as defined in Equation (8). The Fock bras can then be expressed in terms of the operator bras  $|\Pi_j\rangle$  as  $\mathbf{v} = \mathbf{B}_{s,\epsilon}^{-1} \mathbf{V}$ . This compact form proves useful when evaluating the operator trace of the inverted frame operator  $\mathcal{F}^{-1}$ :

$$\text{tr}\{\mathcal{F}^{-1}\} = \text{tr}\{\mathcal{F}^{-1} \mathbf{v}^\dagger \mathbf{v}\} = \text{tr}\{\mathcal{F}^{-1} \mathbf{V}^\dagger \mathbf{B}_{s,\epsilon}^\dagger \mathbf{B}_{s,\epsilon}^{-1} \mathbf{V}\}. \tag{30}$$

At this stage, we emphasize the distinction between the operators (such as  $\mathcal{F}$  and  $|\Pi_j\rangle \langle \Pi_j|$ ) and the columns of (operator) kets (such as  $\mathbf{v}$  and  $\mathbf{V}$ ) to avoid confusion regarding the role of the operator trace  $\text{tr}\{\cdot\}$ . With that, using the basic fact

$$\langle \Pi_j | \mathcal{F}^{-1} | \Pi_k \rangle = \text{tr}\{\Pi_j\} \delta_{j,k} \tag{31}$$

for any minimal POVM, the answer

$$\text{tr}\{\mathcal{F}^{-1}\} = \sum_{j=0}^{d-1} \text{tr}\{\Pi_j\} (\mathbf{B}_{s,\epsilon} \mathbf{B}_{s,\epsilon}^\dagger)_{jj}^{-1} \tag{32}$$

is immediate and

$$\text{TTF}_{\text{multiport}}(s, \{\eta_j\}) = \frac{1}{d} \left[ \sum_{j=0}^{d-1} \text{tr}\{\Pi_j\} (\mathbf{B}_{s,\epsilon} \mathbf{B}_{s,\epsilon}^\dagger)_{jj}^{-1} - \frac{1}{\text{tr}\{\Pi_{d-1}\}} - \frac{2(d-1)}{d+1} \right]. \tag{33}$$

### 5. Multiport Device of Equal Port Efficiencies and $s \rightarrow \infty$ Output Ports

To gain some physical insights from the structure of multiport devices, we begin with a systematic study of the special case where  $\eta_j = \eta$ . With this, Equation (4) immediately applies. Upon an introduction of the simple relation

$$[1 - \eta(s-k)]^n = \left( \frac{\partial}{\partial t} \right)^n e^{t[1 - \eta(s-k)]} \Big|_{t=0}, \tag{34}$$

subsequent analysis may be facilitated after rewriting the POVM amplitudes as

$$\beta_{jn} = \binom{s}{j} \left( \frac{\partial}{\partial t} \right)^n \left[ e^{t(1-\eta s)} (e^{t\eta} - 1)^j \right] \Big|_{t=0}. \tag{35}$$

This formula, which is valid for any  $s$  and  $\eta$ , shall serve as a good starting point for deriving our main results.

5.1. Perfect Multiport Devices Without Losses

If the loss probability is zero ( $\epsilon = 0$ ), the port efficiencies are then all equal to  $\eta = 1/s$ . It follows from Equation (35), that

$$\beta_{jn} = \binom{s}{j} \left( \frac{\partial}{\partial t} \right)^n \left( e^{\frac{t}{s}} - 1 \right)^j \Big|_{t=0} = \frac{j!}{s^n} \binom{s}{j} \left\{ \begin{matrix} n \\ j \end{matrix} \right\}, \tag{36}$$

after an invocation of the moment-generating formula

$$\frac{1}{a^n j!} \left( \frac{\partial}{\partial t} \right)^n \left( e^{at} - 1 \right)^j \Big|_{t=0} = \left\{ \begin{matrix} n \\ j \end{matrix} \right\} \tag{37}$$

for the Stirling number of the second kind  $\left\{ \begin{matrix} n \\ j \end{matrix} \right\}$ . The combinatorial sum rule

$$\sum_{j=0}^n \frac{s!}{(s-j)!} \left\{ \begin{matrix} n \\ j \end{matrix} \right\} = s^n, \tag{38}$$

guarantees the proper normalization of  $\beta_{jn}$  as it should.

For infinitely many ports ( $s \rightarrow \infty$ ), the ratio  $s!/(s-j)! \rightarrow s^j$  and the amplitudes

$$\beta_{jn} \rightarrow \frac{1}{s^{n-j}} \left\{ \begin{matrix} n \\ j \end{matrix} \right\} \Big|_{s \rightarrow \infty} = \delta_{j,n} \tag{39}$$

become those of the Fock states. Put differently, as the multiport device grows in size, its functionality approaches that of the pure Fock-state measurement—indirect photon counting approaches direct photon counting in the large- $s$  limit. As the matrix  $\mathbf{B} \equiv \mathbf{B}_{s \rightarrow \infty, \epsilon=0}$  is simply the  $d \times d$  identity matrix, the TTF takes the value

$$\text{TTF}_{\text{multiport}} \left( s \rightarrow \infty, \left\{ \eta_j = \frac{1}{s} \right\} \right) = \frac{(d-1)^2}{d(d+1)}. \tag{40}$$

As  $d$  increases, the TTF approaches unity. It can be shown that the performance  $\text{TTF}_{\text{multiport}}(s, \{\eta_j\})$  of any arbitrary lossless multiport device is bounded from below by this Fock-state limit (see Appendix A).

5.2. Imperfect Multiport Devices with Losses

When photon losses are present [ $\epsilon > 0, \eta = (1 - \epsilon)/s$ ], Equation (35) gives

$$\beta_{jn} = \binom{s}{j} \left( \frac{\partial}{\partial t} \right)^n \left\{ e^{t\epsilon} \left[ e^{\frac{t}{s}(1-\epsilon)} - 1 \right]^j \right\} \Big|_{t=0}. \tag{41}$$

In the limit  $s \rightarrow \infty$ , the approximation  $e^y \approx 1 + y$  for small  $y$  and  $s!/(s-j)! \rightarrow s^j$  render

$$\begin{aligned} \beta_{jn} &\rightarrow \frac{(1-\epsilon)^j}{j!} \left( \frac{\partial}{\partial t} \right)^n \left( t^j e^{t\epsilon} \right) \Big|_{t=0} = \frac{(1-\epsilon)^j}{j!} \sum_{l=0}^{\infty} \frac{\epsilon^l}{l!} \underbrace{\left( \frac{\partial}{\partial t} \right)^n t^{j+l} \Big|_{t=0}}_{= n! \delta_{l,n-j}} \\ &= \binom{n}{j} (1-\epsilon)^j \epsilon^{n-j} = (\mathbf{B}_\epsilon)_{jn}. \end{aligned} \tag{42}$$



The expression for  $B_\epsilon$  was defined earlier in [26] as a separate consequence of multiphoton losses, the argument of which is independent of taking the limit  $s \rightarrow \infty$ . These amplitudes correspond to those of a POVM comprising binomial mixtures of Fock-state outcomes

$$\Pi_j = \sum_{m=j}^{d-1} |m\rangle \binom{m}{j} (1-\epsilon)^j \epsilon^{m-j} \langle m|, \tag{43}$$

which tends to the set of Fock states in the limits  $\epsilon \rightarrow 0$  and  $d \rightarrow \infty$ . Thus for large multiphoton devices, the probabilities are primarily influenced by the number of detection and absorption events.

To calculate the TTF, we need the inverse of  $B_\epsilon \equiv B_{s \rightarrow \infty, \epsilon}$ , which can be deduced to be

$$B_\epsilon^{-1} = \sum_{j=0}^{d-1} \sum_{n=0}^{d-1} e_j e_n \binom{n}{j} (1-\epsilon)^{-n} (-\epsilon)^{n-j} \tag{44}$$

by a reverse engineering of the binomial theorem. One can effortlessly verify the following obvious necessary property  $B_\epsilon^{-1} B_\epsilon = \mathbf{1}$ . The remaining task is to simply calculate the matrix elements of  $(B_\epsilon B_\epsilon^T)^{-1}$ :

$$\begin{aligned} (B_\epsilon B_\epsilon^T)^{-1}_{jj'} &= \sum_{n=0}^{d-1} \binom{j}{n} (1-\epsilon)^{-j} (-\epsilon)^{j-n} \binom{j'}{n} (1-\epsilon)^{-j'} (-\epsilon)^{j'-n} \\ &= \left(-\frac{\epsilon}{1-\epsilon}\right)^{j'+j} \sum_{n=0}^{d-1} \binom{j}{n} \binom{j'}{n} \frac{1}{\epsilon^{2n}} \\ &= \left(-\frac{\epsilon}{1-\epsilon}\right)^{j'+j} {}_2F_1\left(-j, -j'; \frac{1}{\epsilon^2}\right), \end{aligned} \tag{45}$$

where we have considered a definition

$$\sum_{n=0}^{j <} \binom{j}{n} \binom{j'}{n} y^n = {}_2F_1\left(-j, -j'; 1; y\right), \quad j < = \min\{j, j'\}, \tag{46}$$

for the special case of the Gaussian hypergeometric function  ${}_2F_1\left(\begin{smallmatrix} a_1 & a_2 \\ b_1 \end{smallmatrix}; y\right)$ .

Furthermore, in terms of the regularized incomplete beta function  $I_z(a, b)$ , the operator traces for this multiphoton POVM

$$\text{tr}\{\Pi_j\} = \frac{1}{1-\epsilon} [1 - I_\epsilon(d-j, j+1)]. \tag{47}$$

Notably, we have  $\text{tr}\{\Pi_{d-1}\} = (1-\epsilon)^{d-1}$ , which can be obtained either by

$${}_2F_1\left(\begin{smallmatrix} 1 & d+1 \\ 2 \end{smallmatrix}; y\right) = \frac{1}{dy} \left[ \frac{1}{(1-y)^d} - 1 \right] \tag{48}$$

or the simple physical reasoning that the registration of  $j$  clicks must at least originate from the presence of  $j$  photons ( $j \leq n$ ). A substitution of this final piece of information as well as Equation (45) into Equation (33) leads to

$$\begin{aligned} &\text{TTF}_{\text{multiphoton}}\left(s \rightarrow \infty, \left\{\eta_j = \frac{1-\epsilon}{s}\right\}\right) \\ &= \frac{1}{d} \left[ \sum_{j=0}^{d-1} \text{tr}\{\Pi_j\} \left(\frac{\epsilon}{1-\epsilon}\right)^{2j} {}_2F_1\left(-j, -j; \frac{1}{\epsilon^2}\right) - \frac{1}{(1-\epsilon)^{d-1}} - \frac{2(d-1)}{d+1} \right]. \end{aligned} \tag{49}$$

It is clear that  $\epsilon = 0$  brings us back to the optimal result stated in Equation (40) by noting that

$$\epsilon^{2j} {}_2F_1\left(\begin{matrix} -j & -j \\ 1 \end{matrix}; \frac{1}{\epsilon^2}\right)\Bigg|_{\epsilon=0} = 1 \tag{50}$$

that arises from the definition in Equation (46).

Figure 1 demonstrates the fit between the theoretically predicted TTF values with Equation (49) and the numerically calculated ones after performing Monte–Carlo averaging of the inverse of the Fisher operator  $F(\rho)^{-1}$  (see Equation (19)) over the Haar measure of pure states. To this average numerically, it is sufficient to generate a sufficiently large number of random pure states  $\{\rho_j = \mathcal{A}_j^\dagger \mathcal{A}_j / \text{tr}\{\mathcal{A}_j^\dagger \mathcal{A}_j\}\}$  parametrized by the random complex auxiliary rank-one operators  $\mathcal{A}_j$  that follow the standard Gaussian distribution and use them to compute the average of  $F(\rho)^{-1}$ .

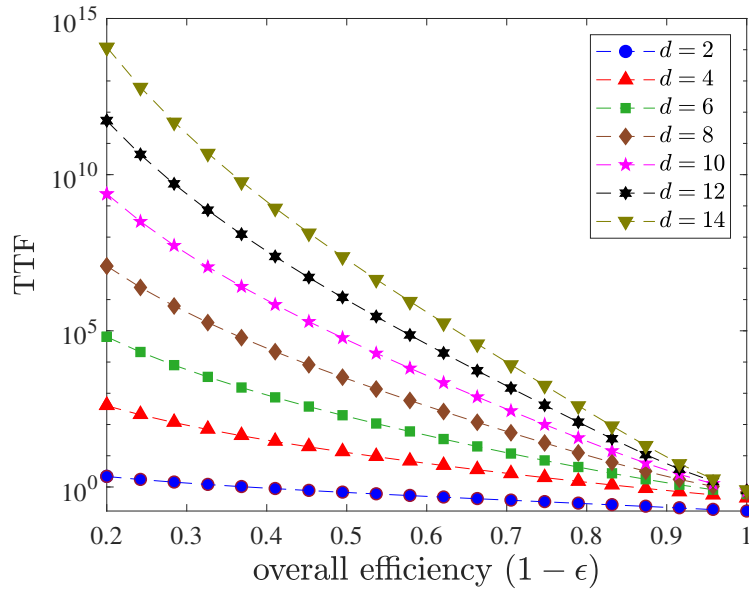


**Figure 1.** Numerical (colored markers) and theoretical (colored dashed curves) values of TTF (logarithmically scaled) for infinitely large multiport devices of various  $\epsilon$  and Hilbert-space dimensions  $d$ . A total of 1000 random pure states were used to evaluate each numerical plot point. The convergence to the optimal TTF in Equation (40) at  $\epsilon = 1$  is as expected. It therefore comes as no surprise that losses monotonically lowers reconstruction accuracy.

### 5.3. Noisy Photon-Number Resolution of Multiport Devices with $s \rightarrow \infty$ and $\epsilon > 0$

In the hypothetical situation where the photon-loss rate  $\epsilon = 0$ , the multiport device is capable of resolving photon numbers in an optical signal described by  $\rho$  of any arbitrary dimension  $d$  (recall that  $d - 1$  is then the maximum number of photons in the signal). We say that the  $d$ -dimensional Hilbert space is resolvable. Therefore any subspace of dimension  $d_{\text{res}} \leq d$  is by definition also resolvable. In real experiments however, a nonzero photon-loss rate directly limits the number of photons resolvable. The key relation that governs this restriction for  $s \rightarrow \infty$  is Equation (47). For a fixed  $d$ ,  $\text{tr}\{\Pi_j\}$  (or  $\Pi_j$ ) becomes essentially zero above certain threshold  $j = j_{\text{thres}}$ . This threshold value defines the dimension of the maximally resolvable subspace— $d_{\text{res}} \leq j_{\text{thres}+1}$ .

More specifically, we may define  $j_{\text{thres}}$  as the largest integer for which

$$1 - I_\epsilon(d - j_{\text{thres}}, j_{\text{thres}} + 1) > \mu_{\text{thres}} \approx 0, \tag{51}$$

where  $\mu_{\text{thres}}$  is a very small positive number close to zero. While this equation has no general analytical solution for finite  $d$ , we note that for large  $d$ ,  $I_\epsilon(d - j, j + 1) \approx \frac{1}{2} + \frac{1}{2} \tanh(j - d(1 - \epsilon))$  is a remarkably

good approximation. We may then use this to derive the simplified and approximate photon-number resolvability restriction

$$d_{\text{res}} \leq d(1 - \epsilon) + \tanh^{-1}(1 - 2\mu_{\text{thres}}). \tag{52}$$

This observation impacts how we should perform asymptotic TTF analyses for multiport devices in the large  $d$ -limit. Unlike the ideal case where one simply takes  $d \rightarrow \infty$  with Equation (40) to arrive at the finite value 1, this naive limit results in the divergence of  $\text{TTF}_{\text{multiport}}$  for any finite  $\epsilon$ . A careful thought reveals that indeed, for the tomography of photon-number distributions for dimension  $d$  to be IC, we require the necessary condition that  $\epsilon$  be no greater than some critical value beyond which the inequality  $1 - I_\epsilon(1, d) > \mu_{\text{thres}}$  becomes invalid. This condition may be approximately written as

$$\epsilon \leq \tanh^{-1}(1 - 2\mu_{\text{thres}})/d \tag{53}$$

for sufficiently large  $d$  following Equation (52). Figures 2 and 3 show the important plots that characterize the informational completeness of any given (infinitely large) multiport device of nonzero photon-loss rate  $\epsilon$ .

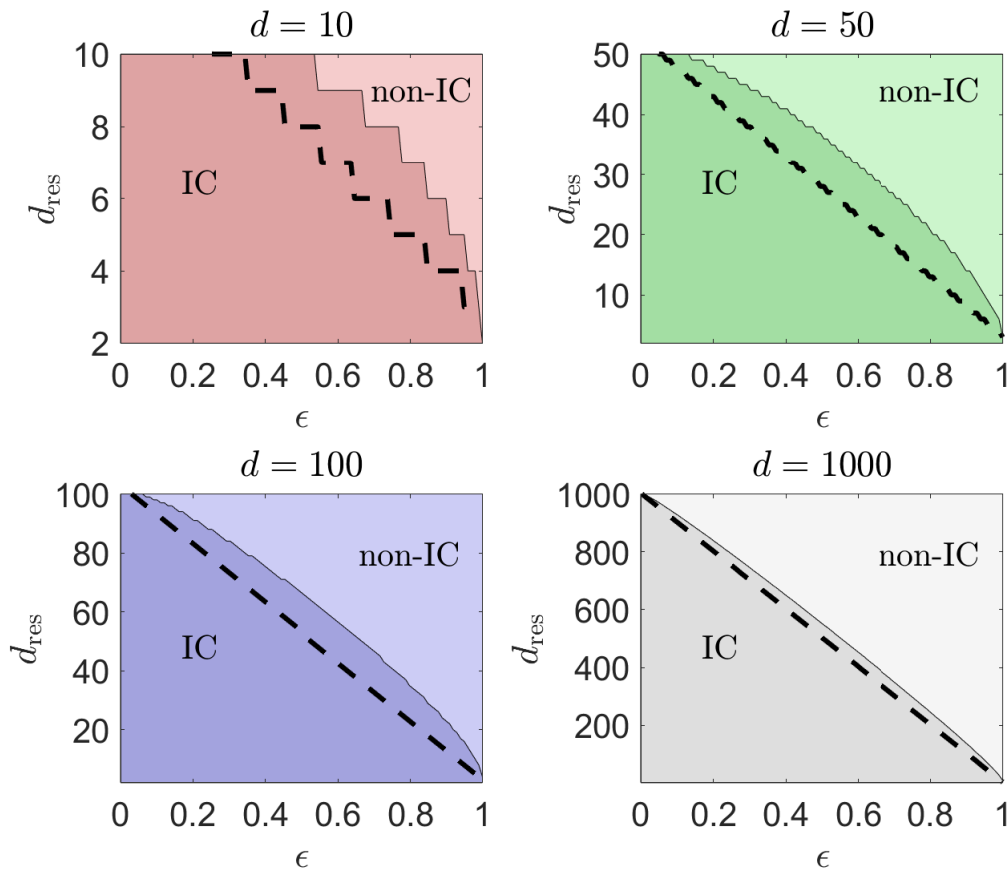


**Figure 2.** Informational completeness phase diagrams for various  $d$  in the  $d_{\text{res}}-\epsilon$  plane with  $\mu_{\text{thres}} = 10^{-3}$ . Subspaces of dimensions below the boundary are resolvable, and hence render the multiport device of  $s \rightarrow \infty$  and  $\eta_j = (1 - \epsilon)/s$  IC. Those of dimensions above the boundary are unresolvable with such a multiport device. The thick dashed curves represent the analytically calculated boundaries using the approximation in (52), which provide conservative underestimates for the maximum  $d_{\text{res}}$  compared to the numerically computed boundaries. Clearly, the range of  $\epsilon$  for which the entire  $d$ -dimensional Hilbert space is completely resolvable reduces as  $d$  increases.

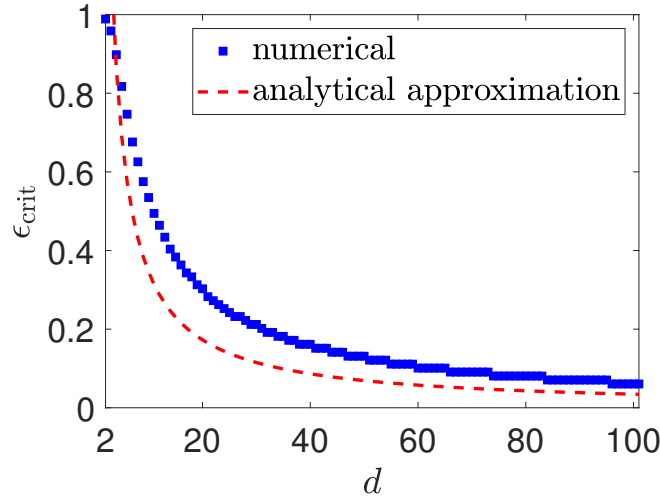


**Figure 3.** A plot of the critical  $\epsilon$  value ( $\epsilon_{\text{crit}}$ ) against  $d$  that shows the maximum amount of photon losses a multiport device can tolerate before losing its informational completeness property. Here,  $\mu_{\text{thres}} = 10^{-3}$ . The simple  $\epsilon_{\text{crit}} \sim 1/d$  behavior serves as a back-of-the-envelope solution for designing such devices.

### 6. Multiport Device of Equal Port Efficiencies and $s$ Output Ports

#### 6.1. Perfect Multiport Devices without Losses

The consideration of a finite-size multiport device with  $s$  output ports more closely resembles the real physical situation in the laboratory in which the resources that go into its implementation are limited. Even in this case, one can still easily compute the TTF for the  $\epsilon = 0$  case where losses are absent in the device. Starting with the POVM amplitudes  $\beta_{jn}$  in Equation (36), we find that the inverse of their corresponding  $\mathbf{B}_s \equiv \mathbf{B}_{s,\epsilon=0}$  amplitude matrix is simply given by

$$\mathbf{B}_s^{-1} = \sum_{j=0}^{d-1} \sum_{n=0}^{d-1} \mathbf{e}_j \mathbf{e}_n \frac{(s-n)!}{s!} s^j (-1)^{n-j} \begin{bmatrix} n \\ j \end{bmatrix} \quad (54)$$

and we owe this simple inversion formula to the existence of the (unsigned) Stirling number of the first kind  $\begin{bmatrix} n \\ j \end{bmatrix}$  that is orthogonal to the Stirling number of the second kind  $\left\{ \begin{matrix} n \\ j \end{matrix} \right\}$  in the sense that

$$\sum_{n=j}^k (-1)^{n-k} \left\{ \begin{matrix} n \\ j \end{matrix} \right\} \begin{bmatrix} k \\ n \end{bmatrix} = \sum_{n=j}^k (-1)^{n-j} \left\{ \begin{matrix} k \\ n \end{matrix} \right\} \begin{bmatrix} n \\ j \end{bmatrix} = \delta_{j,k}. \quad (55)$$

This means that

$$\begin{aligned} (\mathbf{B}_s \mathbf{B}_s^T)^{-1}_{jj'} &= (-1)^{j+j'} \frac{(s-j)!(s-j')!}{s!^2} \sum_{n=0}^{d-1} s^{2n} \begin{bmatrix} j \\ n \end{bmatrix} \begin{bmatrix} j' \\ n \end{bmatrix} \\ &= (-1)^{j+j'} \frac{(s-j)!(s-j')!}{s!^2} {}_2F_1^{(s1)} \left( \begin{matrix} -j & -j' \\ 1 \end{matrix}; s^2 \right), \end{aligned} \quad (56)$$

where we have defined the *Stirling–Gaussian hypergeometric function of the first kind*

$$\sum_{n=0}^{j <} \begin{bmatrix} j \\ n \end{bmatrix} \begin{bmatrix} j' \\ n \end{bmatrix} y^n = {}_2F_1^{(s1)} \left( \begin{matrix} -j & -j' \\ 1 \end{matrix}; y \right) \quad (57)$$

that is of analogous form to the usual Gaussian hypergeometric function in Equation (46). Accordingly, the Stirling–Gaussian hypergeometric function of the second kind  ${}_2F_1^{(s2)}\left(\begin{matrix} -j & -j' \\ 1 \end{matrix}; y\right)$  would then simply involve the Stirling numbers of the second kind.

The resulting performance certifier

$$\begin{aligned} & \text{TTF}_{\text{multiport}}\left(s, \left\{\eta_j = \frac{1}{s}\right\}\right) \\ &= \frac{1}{d} \left\{ \sum_{j=0}^{d-1} \frac{(s-j)!}{s!} {}_2F_1^{(s1)}\left(\begin{matrix} -j & -j \\ 1 \end{matrix}; s^2\right) \sum_{n'=j}^{d-1} \frac{1}{s^{n'}} \left\{ \begin{matrix} n' \\ j \end{matrix} \right\} - \frac{s^{d-1}(s-d+1)!}{s!} - \frac{2(d-1)}{d+1} \right\} \quad (58) \end{aligned}$$

allows us to evaluate the reconstruction accuracy for a finite-size multiport device of equal port efficiencies. As a verification of the validity of Equation (58), we compare it with numerically computed TTF for a sufficiently large set of random pure states distributed to the Haar measure (see Figure 4). Specifically, we note that for  $d = 2$ , the TTF is a constant value of  $1/6$ , which tells us that for effective single-photon sources a two-port device functions exactly like a Fock-state measurement. This can be easily understood in hindsight by realizing that the only POVM outcomes that matter in this subspace are the vacuum and  $n = 1$  Fock states in the absence of losses. All other  $s - 1$  outcomes are not measured.

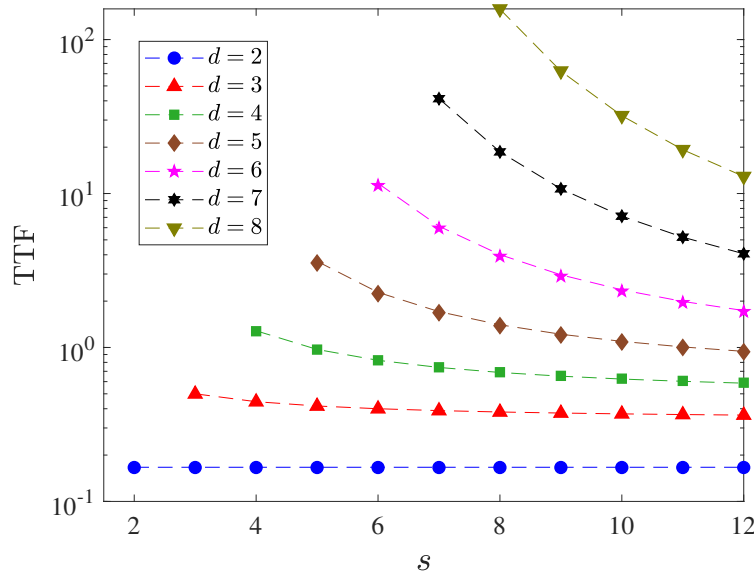


**Figure 4.** Numerical (colored markers) and theoretical (colored dashed curves) values of the TTF (logarithmically scaled) for finite-size multiport devices of various  $s$  values and Hilbert-space dimensions  $d$ . A total of 2000 random pure states were used to evaluate each numerical plot point. The  $s \geq d$  regime illustrates the TTF for IC multiport POVMs only, which is the regime an observer would be interested in for the purpose of photon-number-distribution tomography.

### 6.2. Imperfect Multiport Devices with Losses

The rather specialized physical and mathematical structures of multiport devices permit us to obtain an analytical expression for the TTF even in the most general case where  $s < \infty$  and  $\epsilon > 0$ . The corresponding  $\mathbf{B}_{s,\epsilon}$  for such multiport POVMs can again be inverted by the observation that  $\mathbf{B}_{s,\epsilon} = \mathbf{B}_s \mathbf{B}_\epsilon$ . In other words, a finite-size photoabsorptive multiport device is a device convolution of a perfect finite-size multiport device and photoabsorption losses. This is because

$$\begin{aligned}
 (\mathbf{B}_s \mathbf{B}_\epsilon)_{jn} &= e^n \binom{s}{j} \sum_{n'=0}^n \binom{n}{n'} \left( \frac{1}{\epsilon} \frac{\partial}{\partial t} \right)^{n'} \left[ e^{\frac{t(1-\epsilon)}{s}} - 1 \right] \Big|_{t=0}^j \\
 &= (-1)^j \binom{s}{j} \sum_{k=0}^j \binom{j}{k} (-1)^k \left( \epsilon + \frac{1-\epsilon}{s} k \right)^n \\
 &= (-1)^j \binom{s}{j} \sum_{k=0}^j \binom{j}{k} (-1)^k [1 - \eta(s-k)]^n = (\mathbf{B}_{s,\epsilon})_{jn}.
 \end{aligned} \tag{59}$$

This decomposition implies that  $\mathbf{B}_{s,\epsilon}^{-1} = \mathbf{B}_\epsilon^{-1} \mathbf{B}_s^{-1}$ , so that utilizing the results from Equations (44) and (54) for the two respective components, we can summarize the expressions for the performance measure:

$$\begin{aligned}
 \text{TTF}_{\text{multiport}} \left( s, \left\{ \eta_j = \frac{1-\epsilon}{s} \right\} \right) &= \frac{1}{d} \left[ \sum_{j=0}^{d-1} \text{tr}\{\Pi_j\} (\mathbf{W}_{s,\epsilon}^T \mathbf{W}_{s,\epsilon})_{jj} - \frac{1}{\text{tr}\{\Pi_{d-1}\}} - \frac{2(d-1)}{d+1} \right], \\
 \mathbf{W}_{s,\epsilon} \Big|_{jn} &= (-1)^{n-j} \epsilon^{-j} \frac{(s-n)!}{s!} \sum_{l=j}^n \left( \frac{\epsilon s}{1-\epsilon} \right)^l \binom{l}{j} \begin{bmatrix} n \\ l \end{bmatrix}.
 \end{aligned} \tag{60}$$

Once more, we notice the constant TTF for  $d = 2$  with a value of  $(1 + 2\epsilon)/(6 - 6\epsilon)$  due to the  $s$ -independent multiport POVM consisting of the outcomes

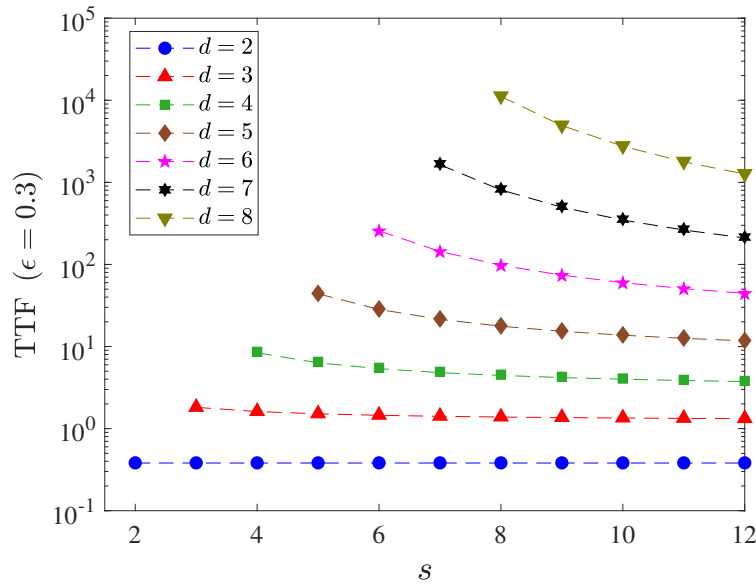
$$\begin{aligned}
 \Pi_0 &= |0\rangle \langle 0| + |1\rangle \epsilon \langle 1|, \\
 \Pi_1 &= |1\rangle (1-\epsilon) \langle 1|.
 \end{aligned} \tag{61}$$

Figure 5 gives the comparison between theory and numerical computations for a sample  $\epsilon$ .

### 6.3. Noisy Photon-Number Resolution of Multiport Devices with $s < \infty$ and $\epsilon > 0$

As with the case of  $s \rightarrow \infty$  in Section 5.3, a nonzero photon-loss rate  $\epsilon$  for a finite-size multiport device also reduces the number of photons that can be resolved. Therefore,  $\epsilon$  should again be smaller than some critical value in order for the multiport device to characterize the complete  $d$ -dimensional photon-number distribution. This critical value may be computed, for every given value of  $s$ , according to the constraint  $\sum_{n=0}^{d-1} (\mathbf{B}_{s,\epsilon})_{d-1,n} > \mu_{\text{thres}} \approx 0$  that is to be satisfied by the largest value of  $\epsilon$ .

In general, the critical value of  $\epsilon$  has no easy analytical form. It is however numerically efficient to plot graphs of the critical values with respect to  $d$  for any physically reasonable  $s$ . Figure 6 shows some sample plots.



**Figure 5.** Numerical (colored markers) and theoretical (colored dashed curves) values of the TTF (logarithmically scaled) for finite-size multiport devices of various  $s$  values, a fixed  $\epsilon = 0.3$ , and Hilbert-space dimensions  $d$ . A total of 2000 random pure states were used to evaluate each numerical plot point. As in the case of  $\epsilon = 0$ , the TTF for  $d = 2$  takes a constant value of 0.3809 for this particular  $\epsilon$  value. The worsening of the tomographic performance with a finite loss probability is clearly manifested as an overall increase in the TTF values.

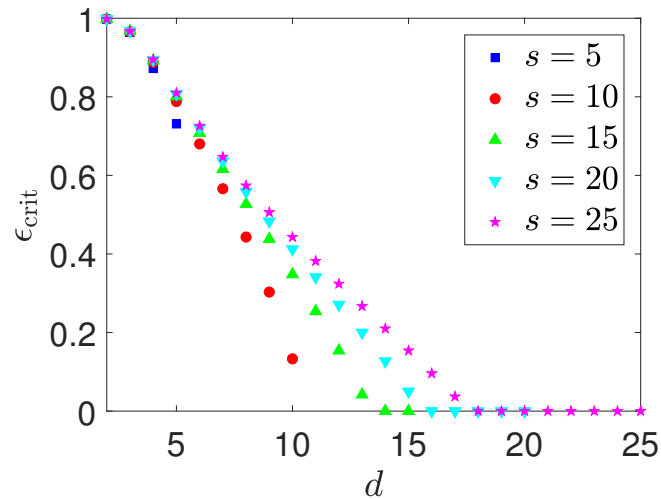


**Figure 6.** A plot of the critical  $\epsilon$  value ( $\epsilon_{\text{crit}}$ ) against  $d$  for various number of outputs  $s$  of the multiport device. The threshold  $\mu_{\text{thres}} = 10^{-3}$  is chosen. For a given  $d$ -dimensional Hilbert subspace, increasing  $s$  also raises  $\epsilon_{\text{crit}}$ , although for reasonable values of  $s$  such an increase is not dramatic even when  $d \ll s$ .

### 7. Discussion

We present a short series of studies related to the performance of multiport devices on photon-number distribution tomography. The central measure of performance is the quantum tomographic transfer function—the uniform average of the inverse Fisher information over all photon-number distributions in the probability simplex.

The mathematical framework for calculating the transfer function introduced in this article allows us to conclude that sufficiently-large multiport devices of equal transmissivity for each output port

function either like a Fock-state measurement or binomial mixtures of Fock-state measurements respectively in the absence and presence of photon losses. These are followed by analytical treatments for finite-size multiport devices. In the presence of photon losses, we have studied and mapped out conditions concerning the photon-number resolving power of noisy multiport devices of both infinite and finite sizes. We show that devices of high photon losses possess weak photon-number resolving power and increasing the number of output ports may help only to a certain limited extent. The optimization of photodetectors and other optical components, especially for the purpose of curbing photon losses, is therefore crucial for building realistic multiport devices for indirect photon counting.

**Author Contributions:** Conceptualization, Y.S.T. and J.Ř.; methodology, Y.S.T.; software, Y.S.T.; validation, Y.S.T. and J.Ř.; formal analysis, Y.S.T.; investigation, Y.S.T.; resources, Y.S.T.; data curation, Y.S.T.; writing—original draft preparation, Y.S.T.; writing—review and editing, Y.S.T., H.J., J.Ř., Z.H., L.L.S.-S., and C.S.; visualization, Y.S.T.; supervision, Y.S.T., H.J., L.L.S.-S., and C.S.; project administration, Y.S.T., H.J., and L.L.S.-S.; funding acquisition, Y.S.T., H.J., J.Ř., Z.H., and L.L.S.-S.

**Funding:** We acknowledge financial support from the BK21 Plus Program (Grant No. 21A2013111123) funded by the Ministry of Education (MOE, Korea) and National Research Foundation of Korea (NRF), the NRF grant funded by the Korea government (MSIP) (Grant No. NRF-2019R1H1A3079890), the Spanish MINECO (Grant No. FIS2015-67963-P and PGC2018-099183-B-I00), the Grant Agency of the Czech Republic (Grant No. 18-04291S), and the IGA Project of the Palacký University (Grant No. IGA PrF 2019-007).

**Conflicts of Interest:** The authors declare no conflict of interest. The funders had no role in the design of the study; in the collection, analyses, or interpretation of data; in the writing of the manuscript, or in the decision to publish the results.

## Appendix A. Optimality of the Fock-State Measurement for Noiseless Multiport Devices

We expect the commuting Fock-state measurement to be the optimal noiseless measurement for photon-number-distribution reconstruction. This expectation can be confirmed by showing that the value of the TTF in Equation (40) is indeed the optimal limit for all multiport devices. To this end, we exploit the inequalities

$$\text{tr}\{AB\} \leq \text{tr}\{A\}\text{tr}\{B\} \quad \text{for } A \geq 0 \text{ and } B \geq 0, \quad (\text{A1})$$

$$\text{tr}\{A\}\text{tr}\{A^{-1}\} \geq \dim\{A\}^2 \quad \text{for any invertible } A, \quad (\text{A2})$$

and remind ourselves that the TTF expression in Equation (33) holds for any  $s$ ,  $\{\eta_j\}$  and  $\epsilon$ . As the operator trace

$$\text{tr}\{\mathcal{F}\} = \sum_{j=0}^{d-1} \frac{\text{tr}\{\Pi_j^2\}}{\text{tr}\{\Pi_j\}} \leq \sum_{j=0}^{d-1} \text{tr}\{\Pi_j\} = \text{tr}\{1\} = d \quad (\text{A3})$$

of the general frame operator is bounded from above according to (A1), the inequality in (A2) implies that

$$\text{tr}\{\mathcal{F}^{-1}\} \geq d. \quad (\text{A4})$$

Together with the obvious fact that the probability of detecting all available photons from the input signal never exceeds one ( $\text{tr}\{\Pi_{d-1}\} \leq 1$ ), we have the general inequality

$$\text{TTF}_{\text{multiport}}(s, \{\eta_j\}) \geq \text{TTF}_{\text{multiport}}\left(s \rightarrow \infty, \left\{\eta_j = \frac{1}{s}\right\}\right) \quad (\text{A5})$$

to confirm that the Fock-state measurement condition  $\{s \rightarrow \infty, \{\eta_j = 1/s\}\}$  is indeed optimal.



### Appendix B. Averages over the Probability Simplex

We shall give simple derivations of the identities in (24). The general  $m$ -moment integral of interest in our context takes the form

$$I_m = \int_0^1 dp_0 \cdots \int_0^1 dp_{d-1} \delta\left(1 - \sum_{l=0}^{d-1} p_l\right) p_j^m, \tag{A6}$$

in which the simplex constraint  $\sum_{l=0}^{d-1} p_l = 1$  is obeyed. Using the integral representation

$$\delta(x) = \int \frac{dk}{2\pi} e^{ikx} \tag{A7}$$

for the delta function,

$$\begin{aligned} I_m &= \int \frac{dk}{2\pi} e^{ik} \int_0^1 dp_0 \cdots \int_0^1 dp_{d-1} e^{-ik(p_0 + \cdots + p_{d-1})} p_j^m \\ &= \int \frac{dk}{2\pi} e^{ik} \frac{(1 - e^{-ik})^{d-1}}{(ik)^{d-1}} \int_0^1 dp_j e^{-ikp_j} p_j^m \\ &= \int \frac{dk}{2\pi} e^{ik} \frac{(1 - e^{-ik})^{d-1}}{(ik)^{d-1}} \left(i \frac{d}{dk}\right)^m \left[\frac{1}{ik} (1 - e^{-ik})\right], \end{aligned} \tag{A8}$$

where if  $y \equiv ik$ ,

$$\begin{aligned} \left(i \frac{d}{dk}\right)^m \left[\frac{1}{ik} (1 - e^{-ik})\right] &= (-1)^m \left(\frac{d}{dy}\right)^m \left[y^{-1}(1 - e^{-y})\right] \\ &= m! y^{-m-1} (1 - e^{-y}) - \sum_{n=1}^m \frac{m!}{n!} y^{-m+n-1} e^{-y}, \end{aligned} \tag{A9}$$

so that

$$I_m = m! \int \frac{dk}{2\pi} e^{ik} \frac{(1 - e^{-ik})^d}{(ik)^{m+d}} - \sum_{n=1}^m \frac{m!}{n!} \int \frac{dk}{2\pi} \frac{(1 - e^{-ik})^{d-1}}{(ik)^{m-n+d}}. \tag{A10}$$

The first term can be evaluated using the identity

$$\frac{1}{y^{m+1}} = \frac{1}{m!} \int_0^\infty dt t^m e^{-yt}. \tag{A11}$$

This gives

$$\begin{aligned} m! \int \frac{dk}{2\pi} e^{ik} \frac{(1 - e^{-ik})^d}{(ik)^{m+d}} &= \frac{m!}{(m+d-1)!} \sum_{n=0}^d \binom{d}{n} (-1)^n \int_0^\infty dt t^{m+d-1} \underbrace{\int \frac{dk}{2\pi} e^{ik(1-n-t)}}_{= \delta(1-n-t)} \\ &= \frac{m!}{(m+d-1)!} \sum_{n=0}^d \binom{d}{n} (-1)^n \delta_{n,0} \\ &= \frac{m!}{(m+d-1)!}. \end{aligned} \tag{A12}$$

Next, it is possible to argue that the second term of (A10) is zero, since upon repeating the same exercise, we arrive at  $\delta(n+t)$  instead of  $\delta(1-n-t)$  as in the first line of (A12).

Therefore, the  $m$ th moment of  $p_j$  over the probability simplex is

$$\mathbb{E}_{|\rho\rangle}[p_j^m] = \frac{I_m}{I_0} = \binom{m+d-1}{m}^{-1}. \quad (\text{A13})$$

In the regime of  $d \gg m$ , we then have  $\mathbb{E}_{|\rho\rangle}[p_j^m] \approx \frac{\sqrt{2\pi m}}{(ed/m)^m} = O\left(\frac{1}{d^m}\right)$ .

## References

1. Wildfeuer, C.F.; Pearlman, A.J.; Chen, J.; Fan, J.; Migdall, A.; Dowling, J.P. Resolution and sensitivity of a Fabry-Perot interferometer with a photon-number-resolving detector. *Quantum Limits in Optical Interferometry. Phys. Rev. A* **2009**, *80*, 043822. [[CrossRef](#)]
2. Demkowicz-Dobrzański, R.; Jarzyna, M.; Kołodyński, J. Resolution and sensitivity of a Fabry-Perot interferometer with a photon-number-resolving detector. *Prog. Opt.* **2015**, *60*, 345.
3. Von Helversen, M.; Böhm, J.; Schmidt, M.; Gschrey, M.; Schulze, J.-H.; Strittmatter, A.; Rodt, S.; Beyer, J.; Heindel, T.; Reitzenstein, S. Quantum metrology of solid-state single-photon sources using photon-number-resolving detectors. *New J. Phys.* **2019**, *21*, 035007. [[CrossRef](#)]
4. Wu, J.-Y.; Toda, N.; Hofmann, H.F. Observation of squeezed states with strong photon-number oscillations. *Phys. Rev. A* **2009**, *100*, 013814.
5. Cattaneo, M.; Paris, M.G.A.; Olivares, S. Hybrid quantum key distribution using coherent states and photon-number-resolving detectors. *Phys. Rev. A* **2018**, *98*, 012333. [[CrossRef](#)]
6. Stucki, D.; Ribordy, G.; Stefanov, A.; Zbinden, H.; Rarity, J.G.; Wall, T. Photon counting for quantum key distribution with peltier cooled ingaas/inp apds. *J. Mod. Opt.* **2001**, *48*, 1967. [[CrossRef](#)]
7. Kilmer, T.; Guha, S. Boosting linear-optical Bell measurement success probability with predetection squeezing and imperfect photon-number-resolving detectors. *Phys. Rev. A* **2019**, *99*, 032302. [[CrossRef](#)]
8. Ren, M.; Wu, E.; Liang, Y.; Jian, Y.; Wu, G.; Zeng, H. Quantum random-number generator based on a photon-number-resolving detector. *Phys. Rev. A* **2011**, *83*, 023820. [[CrossRef](#)]
9. Applegate, M.J. Efficient and robust quantum random number generation by photon number detection. *Appl. Phys. Lett.* **2015**, *107*, 071106. [[CrossRef](#)]
10. Eisaman, M.D.; Fan, J.; Migdall, A.; Polyakov, S.V. Single-photon sources and detectors. *Rev. Sci. Instrum.* **2011**, *82*, 071101. [[CrossRef](#)]
11. Jönsson, M.; Björk, G. Evaluating the performance of photon-number-resolving detectors. *Phys. Rev. A* **2019**, *99*, 043822. [[CrossRef](#)]
12. Mirin, R.P.; Nam, S.W.; Itzler, M.A. Single-Photon and Photon-Number-Resolving Detectors. *IEEE Photonics J.* **2011**, *4*, 629. [[CrossRef](#)]
13. Marsili, F.; Bitauld, D.; Gaggero, A.; Jahanmirinejad, S.; Leoni, R.; Mattioli, F.; Fiore, A. Physics and application of photon number resolving detectors based on superconducting parallel nanowires. *New J. Phys.* **2009**, *11*, 045022. [[CrossRef](#)]
14. Marsili, F.; Najafi, F.; Dauler, E.; Bellei, F.; Hu, X.; Csete, M.; Molnar, R.J.; Berggren, K.K. Single-Photon Detectors Based on Ultranarrow Superconducting Nanowires. *Nano Lett.* **2011**, *11*, 2048. [[CrossRef](#)] [[PubMed](#)]
15. Jahanmirinejad, S.; Frucci, G.; Mattioli, F.; Sahin, D.; Gaggero, A.; Leoni, R.; Fiore, A. Photon-number resolving detector based on a series array of superconducting nanowires. *Appl. Phys. Lett.* **2012**, *101*, 072602. [[CrossRef](#)]
16. Matekole, E.S.; Vaidyanathan, D.; Arai, K.W.; Glasser, R.T.; Lee, H.; Dowling, J.P. Room-temperature photon-number-resolved detection using a two-mode squeezer. *Phys. Rev. A* **2017**, *96*, 053815. [[CrossRef](#)]
17. Ma, J.; Masoodian, S.; Starkey, D.A.; Fossum, E.R. Photon-number-resolving megapixel image sensor at room temperature without avalanche gain. *Optica* **2017**, *4*, 1474. [[CrossRef](#)]
18. Zolotov, P.; Divochiy, A.; Vakhtomin, Y.; Moshkova, M.; Morozov, P.; Seleznev, V.; Smirnov, K. Photon-number-resolving SSPDs with system detection efficiency over 50 at telecom range. *AIP Conf. Proc.* **2018**, *1936*, 020019.
19. Cai, Y.; Chen, Y.; Chen, X.; Ma, J.; Xu, G.; Wu, Y.; Xu, A.; Wu, E. Metamodelling for Design of Mechatronic and Cyber-Physical Systems. *Appl. Sci.* **2019**, *9*, 2638. [[CrossRef](#)]

20. Paul, H.; Törma, P.; Kiss, T.; Jex, I. Photon Chopping: New Way to Measure the Quantum State of Light. *Phys. Rev. Lett.* **1996**, *76*, 2464. [[CrossRef](#)]
21. Kok, P.; Braunstein, S.L. Detection devices in entanglement-based optical state preparation. *Phys. Rev. A* **2001**, *63*, 033812. [[CrossRef](#)]
22. Rohde, P.P.; Webb, J.G.; Huntington, E.H.; Ralph, T.C. Photon number projection using non-number-resolving detectors. *New J. Phys.* **2007**, *9*, 233. [[CrossRef](#)]
23. Řeháček, J.; Hradil, Z.; Haderka, O.; Peřina J., Jr.; Hamar, M. Multiple-photon resolving fiber-loop detector. *Phys. Rev. A* **2003**, *67*, 061801(R). [[CrossRef](#)]
24. Banaszek, K.; Walmsley, I.A. Fiber-assisted detection with photon number resolution. *Opt. Lett.* **2003**, *28*, 52. [[CrossRef](#)] [[PubMed](#)]
25. Fitch, M.J.; Jacobs, B.C.; Pittman, T.B.; Franson, J.D. Photon-number resolution using time-multiplexed single-photon detectors. *Phys. Rev. A* **2003**, *68*, 043814. [[CrossRef](#)]
26. Achilles, D.; Silberhorn, C.; Sliwa, C.; Banaszek, K.; Walmsley, I.A.; Fitch, M.J.; Jacobs, B.C.; Pittman, T.B.; Franson, J.D. Photon-number-resolving detection using time-multiplexing. *J. Mod. Opt.* **2004**, *51*, 1499. [[CrossRef](#)]
27. Avenhaus, M.; Laiho, K.; Chekhova, M.V.; Silberhorn, C. Accessing Higher Order Correlations in Quantum Optical States by Time Multiplexing. *Phys. Rev. Lett.* **2010** *104*, 063602. [[CrossRef](#)]
28. Kruse, R.; Tiedau, J.; Bartley, T.J.; Barkhofen, S.; Silberhorn, C. Limits of the time-multiplexed photon-counting method. *Phys. Rev. A* **2017**, *95*, 023815. [[CrossRef](#)]
29. Teo, Y.S. *Introduction to Quantum-State Estimation*; World Scientific Publishing Co.: Singapore, 2015.
30. Řeháček J.; Teo, Y.S.; Hradil, Z. Determining which quantum measurement performs better for state estimation. *Phys. Rev. A* **2015**, *92*, 012108. [[CrossRef](#)]



© 2019 by the authors. Licensee MDPI, Basel, Switzerland. This article is an open access article distributed under the terms and conditions of the Creative Commons Attribution (CC BY) license (<http://creativecommons.org/licenses/by/4.0/>).